IEEE Photonics Journal
An IEEE Photonics Society Publication

Photonic Instantaneous Frequency Measurement: Parallel Simultaneous Implementations in a Single Highly Nonlinear Fiber

Volume 3, Number 5, October 2011

L. A. Bui
N. Sarkhosh
A. Mitchell, Member, IEEE

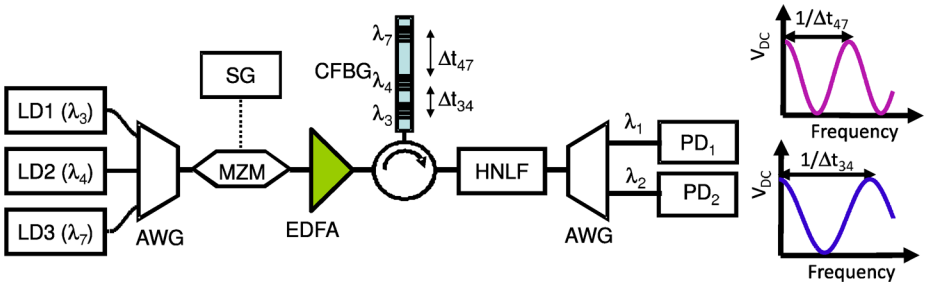

DOI: 10.1109/JPHOT.2011.2169657
1943-0655/$26.00 ©2011 IEEE

Photonic Instantaneous Frequency Measurement: Parallel Simultaneous Implementations in a Single Highly Nonlinear Fiber

L. A. Bui, N. Sarkhosh, and A. Mitchell, *Member, IEEE*

ARC Centre for Ultra-high bandwidth Devices for Optical Systems, School of Electrical and Computer Engineering, Royal Melbourne Institute of Technology (RMIT) University, Melbourne, Vic. 3001, Australia

DOI: 10.1109/JPHOT.2011.2169657
1943-0655/$26.00 ©2011 IEEE

Manuscript received August 11, 2011; revised September 9, 2011; accepted September 15, 2011. Date of publication September 26, 2011; date of current version October 14, 2011. This work was supported by the Australian Research Council through its Centers of Excellence program. Corresponding author: L. A. Bui (e-mail: lam.bui@rmit.edu.au).

Abstract: A microwave photonic system that simultaneously implements multiple parallel instantaneous frequency measurement systems within a single highly nonlinear optical fiber is proposed and practically demonstrated. Three optical carriers of different wavelengths are modulated by the same radio-frequency (RF) signal and then delayed differentially. All three carriers are then mixed within a highly nonlinear optical fiber. The mixing products are separated, and the optical power of each is used to deduce input RF frequency. We demonstrate simultaneous acquisition of two distinct frequency measurement responses over the range from 1 to 40 GHz. This system is all-optical and requires no high-speed electronic components. Avenues for further increasing the number of simultaneous channels are identified.

Index Terms: Microwave photonics, fiber optics links and subsystems, nonlinear optics, four wave mixing.

1. Introduction

Instantaneous frequency measurement (IFM) systems are important elements for many broadband radio-frequency (RF) signal processing systems. IFMs are of particular importance for electronic warfare radar warning receivers, where they can provide a rapid indication of which RF frequency a particular threat is utilizing. This information can guide the efficient and effective application of more sophisticated signal processing resources to accurately identify the threat and trigger the appropriate response. IFM systems implemented using traditional RF technology have excellent performance, even up to 20 GHz. However, these components often rely on traveling wave RF components and high-speed electronic mixers [1], [2], which can incur significant bulk and weight and are also sensitive to electronic attack.

A number of investigations into microwave photonic IFM implementations have been reported as a means of reducing weight and susceptibility to electromagnetic interference. Some examples utilize dispersion induced signal fading [3], double modulation of the optical signal [4], and discrimination on the basis of time of arrival of pulses [5]. Each of these techniques relies on high-speed electronics or the addition of lengths of RF transmission lines.

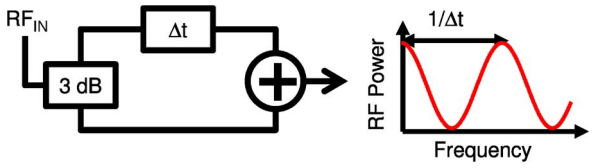

Fig. 1. Principle of an interferometric frequency measurement system.

Recently, we have demonstrated a new photonic IFM system using highly nonlinear optical fiber [6]. This implementation is surprisingly repeatable and stable and does not require high-frequency electronics at any point within the system, alleviating the electronic bottleneck and ensuring that the system is resilient to even extreme electromagnetic environments. Although the reported system offered many advantages, it was realized using a set of relatively expensive photonic components and implemented only a single IFM function. In practice, multiple IFMs should be used in parallel to unambiguously resolve the frequency and amplitude of a measured signal. Thus, the configuration of [6] would be impractically expensive if it were necessary to duplicate the entire system many times. In this paper, we present a new technique by which the system of [6] can implement multiple IFM systems simultaneously using only a single set of photonic components. It should be noted that a preliminary proof of this concept was presented by us in [7], while the current paper provides full implementation details and rigorous analysis.

The paper is organized as follows. Section 2 presents the conceptual background for this research, including the principle of operation of a simple, interferometric IFM system and a review of the previously demonstrated single channel microwave photonic IFM. Section 3 explains the concept of multiple parallel IFM system, and Section 4 presents a proposed system implementation which allows multiple IFM functions with only modest increase in complexity and component count. Experimental results are presented in Section 5. Section 6 provides a discussion, presents conclusions, and suggests directions for further investigation. Finally, the Appendix provides detailed system characterization and derivation of system frequency response measured at DC.

2. Background

A simple, interferometric IFM is presented in Fig. 1. An input RF signal (RF_{IN}) is divided into two equal halves. One half is delayed with respect to the other by a known delay (Δt), and the two differentially delayed signals are then summed and the output power is then measured. Since the time delay is fixed, the phase delay between the two signals will be proportional to the frequency of the input signal, and hence, the output power will oscillate periodically as the input frequency is varied. Through knowledge of the differential delay (Δt), it is possible to interpret the output power received as a measurement of the input RF frequency. The system of Fig. 1 has the advantage of simplicity but requires measurement of RF power at the frequency of the incoming signal, which could be in the millimeter (mm)-wave regime. Accurate measurement over multioctave bandwidths up to mm-wave frequencies can require expensive, broadband electronics. Further, owing to the oscillatory nature of the output response, a number of these systems with different time delays should be used in parallel to unambiguously obtain a high-sensitivity, broad-band frequency measurement that is independent of the signal power.

We have previously implemented a microwave photonic IFM using all-optical mixing [6] which overcomes the need to measure high-frequency RF signals. This system is illustrated in Fig. 2(a). Two optical carriers of different frequency are provided by laser diodes LD1 (ω_1) and LD2 (ω_2) [see Fig. 2(b)]. These carriers are combined, and then, both are modulated by the same RF signal (RF_{IN}), creating sidebands of amplitude equal to the modulation index (m), as shown in Fig. 2(c). The modulated carriers are then separated and differentially delayed accumulating a time difference (Δt) [see Fig. 2(c)]. The two differentially delayed optical signals are then introduced to a highly nonlinear fiber (HNLF) where four wave mixing (FWM) produces idlers at the sum and difference frequencies of the pump frequencies (ω_1 and ω_2), producing new frequencies ($2\omega_1 - \omega_2$ and

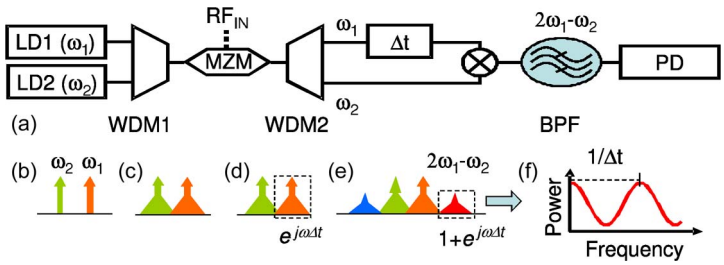

Fig. 2. (a) Principle of operation of a single channel IFM. (b) Lasers LD1 and LD2 generate optical carriers at frequencies ω_1 and ω_2. Arrayed Waveguide Grating (AWG) combines ω_1 and ω_2. (c) Both carriers are modulated by an RF signal using Mach–Zehnder modulator (MZM). (d) ω_1 and ω_2 are separated and differentially delayed by time Δt and then multiplied together using four-wave mixing to create idler at $2\omega_1 - \omega_2$. (e) This idler has power oscillates with RF signal frequency and can be used for frequency measurement.

$2\omega_2 - \omega_1$). For pumps at optical frequencies, while approximate, it is acceptable to consider FWM of two pump wavelengths (λ_1 and λ_2) producing idlers at new wavelengths ($2\lambda_1 - \lambda_2$) and ($2\lambda_2 - \lambda_1$). This approximation is used for the remainder of this paper. These idlers contain components of both delayed and undelayed signals. These components are summed coherently and thus the optical power at these mixing products varies with the relative phase of the mixed carriers.

Since the idlers appear at a different wavelength to the original carriers, they can be isolated using an optical bandpass filter. The total optical power at the idler wavelength (λ_{Idler}) oscillates as a function of the input RF frequency. This oscillation can be measured with a simple DC photodetector with no need to measure the high-frequency signals carried by this optical channel.

A detailed derivation of the theoretically predicted behavior of the nonlinear IFM is presented in [6], where it is shown that the total optical power present around the idler wavelength $(P(\lambda_{\text{Idler}}))$ should be related to the differential time delay and input RF frequency by

$$P(\lambda_{\text{Idler}}) \propto A^2 + B^2[5 + 4\cos(\Omega\Delta t - \psi_1 - \psi_4)] + B^2[5 + 4\cos(\Omega\Delta t - \psi_2 - \psi_3)] \quad (1)$$

where Ω is the RF frequency, A is the power in the optical carrier, and B is the power in the RF sidebands of the signal. The terms ψ_1, ψ_2, ψ_3, and ψ_4 are phase terms corresponding to the dispersion incurred during the differential delay.

Equation (1) predicts that the total idler power will oscillate with input RF frequency, and thus, the idler power measured at the output could be interpreted as a measurement of the input RF frequency. Importantly, the optical phase of the components that are coherently summed at each idler are the product of the optical phases of the two original carriers. Thus, the power measured at the idler is immune to relative optical phase shifts between the two input carriers. Hence, the IFM system is extremely stable.

We have experimentally demonstrated that the system of Fig. 2 can provide broadband frequency measurements from 1 to 40 GHz without requiring any high-speed electronics [6]. However, due to the oscillatory nature of the response, unambiguous measurement can only be made within a frequency range corresponding to a single half period of the oscillating response. To overcome this limitation, several systems with different delays should be operated simultaneously to provide a set of independent measurements from which an unambiguous frequency measurement can be determined. If it was necessary to duplicate the entire system of Fig. 2, then this approach would be impractically bulky and expensive.

3. Parallel IFM System Concept

A system configuration that may allow parallel IFMs to be implemented within a single set of equipment is illustrated in Fig. 3. Here, three optical carriers, each with a different frequency, are combined, and all three are modulated by the same RF signal using a single Mach–Zehnder modulator. The carriers are then separated, and each is subject to a different time delay. The three

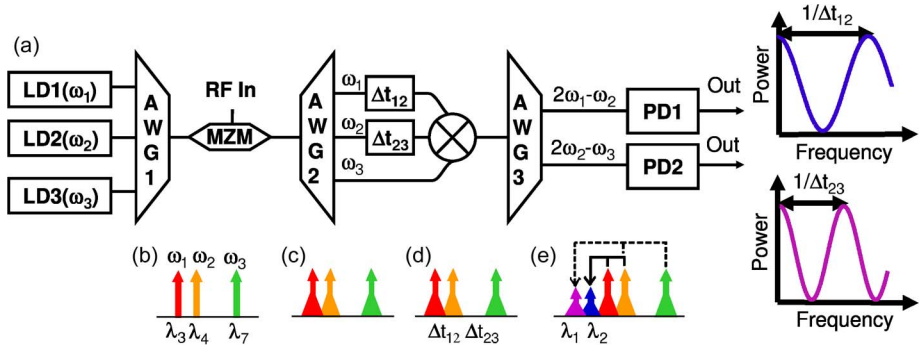

Fig. 3. (a) Concept of multiple parallel IFM measurements. (b) Lasers (LD1, LD2, and LD3) provide optical carriers at frequencies ω_1, ω_2, and ω_3. (c) AWG combines all carriers to the input of MZM, where they are modulated by a single RF signal. (d) The optical signals are then separated and delayed such that the delay differences between ω_1 and ω_2 and between ω_2 and ω_3 are Δt_{12} and Δt_{23}, respectively. The optical carriers are then multiplied together. (e) The idlers of mixing ω_1 and ω_2 and mixing ω_2 and ω_3 are isolated, and their optical powers are measured with DC photodetectors providing two independent frequency measurements of the RF signal. Also included in (b) and (e) are the wavelength labels used for the system demonstration in Section 4.

differentially delayed signals are then recombined and introduced to an HNLF [7], where they are subject to FWM producing many idlers at the sum and difference frequencies of the three original optical carriers. Through careful selection of the three input optical carrier wavelengths, it is possible to generate distinct idlers that contain contributions from only two of the original carriers. These distinct idlers can be isolated using a wavelength-division multiplexer.

Similar to the system of [6], the idlers will comprise the coherent summation of the RF signals from the original carriers, and thus, the optical power measured at each output will depend on the time delay applied to each optical carrier and the RF frequency of the carried signal. However, since there are now different delays between different pairs of the three input carriers, several IFM functions can be achieved simultaneously.

To model the power expected at each idler, we assume that although three carriers are present within the HNLF, our careful choice of frequencies (wavelengths) ensures that that only two carriers contribute to any one idler. If this is the case, then we may simply use (1) to predict the idler power for each pair of the three input carriers. This will result in several independent measurements, mapping intensity to RF input frequency, which can be used to improve sensitivity and frequency range over which unambiguous measurement can be made.

Comparing Figs. 2 and 3, it can be seen that the system component count has only been increased modestly with many of the optical components in Fig. 3 now manipulating multiple wavelengths simultaneously. Thus, in principle, we should be able to implement multiple IFM functions without the requirement of duplicating the entire system, significantly reducing the cost and complexity per IFM implementation. Having proposed a parallel version of our microwave photonic IFM using HNLF, we must now investigate whether this system can practically be achieved.

4. Parallel IFM System Implementation

A diagram of the practical implementation of our simultaneous parallel microwave photonic IFM is presented in Fig. 4. Three optical carriers are provided by laser diodes LD1, LD2, and LD3. All three carriers are combined using an arrayed waveguide grating (AWG, ANDevices DWDM-F-100G) and are simultaneously modulated by a single Mach–Zehnder Modulator (MZM, Micreo/RMIT 40 GHz) with an RF signal provided by a 1–40 GHz signal generator (SG, Anritsu MG3694A). The modulated carriers are then amplified to a total optical power of approximately 20 mW using an Erbium Doped Fiber Amplifier (Pritel PMFA-20-IO). A differential delay is introduced between the carriers by reflecting them from a cascaded fiber Bragg grating (CFBG, Redfern Optical Components) which

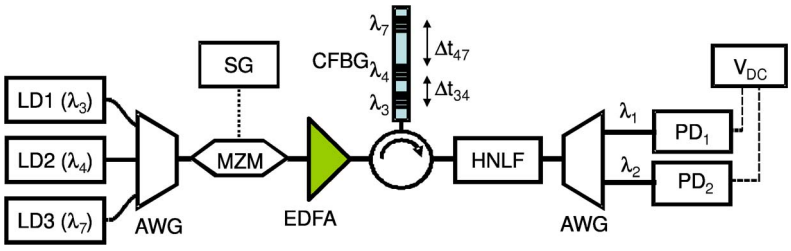

Fig. 4. Experimental setup to demonstrate dual parallel IFMs in a single HNLF.

reflects different wavelengths from different locations along its length. On reflection, a circulator directs the modulated, amplified, and differentially delayed optical carriers to a single HNLF (1 km of OFS Standard HNLF, zero dispersion: 1540 nm, dispersion slope: 0.019 ps$/(\text{nm}^2\text{km})$, and $\gamma = 21/\text{W/km}$), where they co-propagate and generate idlers via FWM. The optical signal is introduced to a second AWG to separate each of the original optical wavelengths, as well as the idlers. The optical powers of two of these isolated idler channels are monitored using DC photodetectors (New Focus 2011) and digital voltmeters. All components up to the HNLF are polarization maintaining to ensure that the optical carriers entering the HNLF were of the same polarization to maximize mixing efficiency.

To demonstrate the system of Fig. 4, the optical wavelengths were chosen to be 1545.2, 1546.9, and 1551.6 nm, respectively. These wavelengths were named λ_3, λ_4, and λ_7, respectively, with reference to the ports of the AWGs, which were used to combine and separate them [see Fig. 3(b)]. On transmission through the HNLF, it was expected that many idlers would be produced at the sum and difference frequencies of these three optical inputs. One idler would be found at λ_2, which had a wavelength of two times λ_3 minus λ_4 [$2 \times 1545.2 - 1546.9 = 1543.5$ nm; see Fig. 3(e)] and thus would contain contributions from these two channels. The careful selection of wavelength of λ_7 ensures that neither the idlers produced by mixing λ_7 and λ_4, nor would those produced by mixing λ_7 and λ_3 appear at λ_2, and thus, the idler at λ_2 would include *only* contributions from λ_3 and λ_4.

Similarly, the wavelength of λ_1 was two times λ_4 minus λ_7 [$2 \times 1546.9 - 1551.6 = 1542.2$ nm; see Fig. 3(e)] but was not at the idler frequency produced by mixing λ_3 and λ_4 or by mixing λ_3 and λ_7, and thus, λ_1 would include *only* contributions from λ_4 and λ_7.

The CFBG produced a differential delay of $\Delta t_{34} \approx 40$ ps between λ_3 and λ_4 and $\Delta t_{47} \approx 120$ ps between channels λ_4 and λ_7. The optical powers at λ_1 and λ_2 were easily isolated using an eight-channel AWG, and the DC optical power on each channel was monitored independently as a function of input RF frequency providing two independent outputs with different oscillation periods which could be used for unambiguous frequency measurement.

To utilize this system for frequency measurement, an accurate prediction of the expected optical power for each input RF frequency must be available to provide amplitude comparison functions (ACFs) for the two IFM implementations. To enable such a prediction, it was necessary to characterize the RF frequency response of each of the various components of the system of Fig. 4. This characterization and calibration of the system of Fig. 4 is somewhat laborious, and thus, these details are presented in the Appendix.

5. Parallel IFM System Demonstration

In the previous section, we have proposed a practical parallel IFM system configuration (see Fig. 4) and have proposed (1) as a theoretical model that will allow prediction the response of this system. We have established a system implementation, and in the Appendix, we have characterized the frequency response of each of the system components and reformulated (1) as (2) such that it can be used as an accurate ACF for frequency measurement. We can thus now demonstrate the implementation of Fig. 4 operating as a frequency measurement system. We have reasoned in Section 4 that due to our careful choice of carrier wavelengths, our output idler signals will be affected only by two of the three input wavelengths. Thus, (2) should be equally valid for predicting

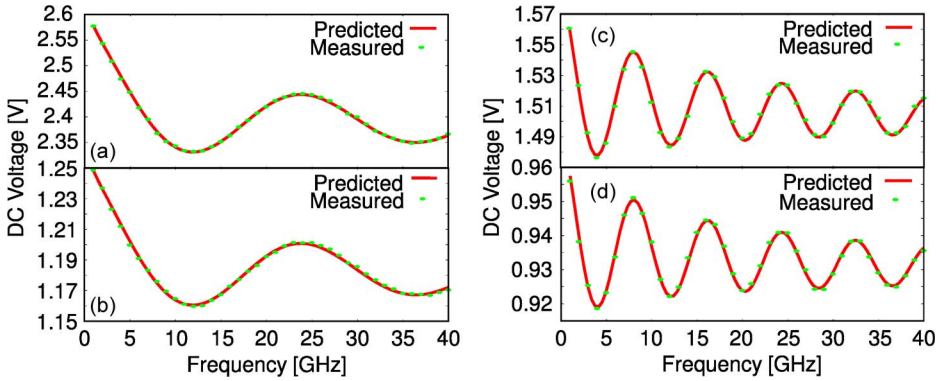

Fig. 5. Measured output DC voltages versus input RF frequency. (a) Voltage at λ_2 for mixing of only two channels (λ_3 and λ_4). (b) Voltage at λ_2 for mixing of three channels (λ_3, λ_4, and λ_7). (c) Voltage at λ_1 for mixing of only two channels (λ_4 and λ_7). (d) Voltage at λ_1 for mixing of three channels (λ_3, λ_4, and λ_7). Solid lines are predictions using (2) and characterization data of the Appendix, and dots are measurements.

the ACF for two or three input wavelengths. To verify this hypothesis, we characterize the system of Fig. 4, first with only pairs of wavelengths and then with all three wavelengths present.

The system of Fig. 4 was configured as described in Section 4, and the frequency provided by the SG was swept from 1 to 40 GHz and the optical power at the output of λ_1 and λ_2 were recorded as a function of this frequency with various combinations of the input wavelengths. The power on each input wavelength channel was maintained equal. When changing which wavelengths were input, the Erbium-doped fiber amplifier (EDFA) gain was adjusted to ensure that the total power entering the HNLF was 20 mW in each case. This modest power level was chosen to minimize the effects of stimulated Brillouin scattering (SBS).

Fig. 5(a) presents the optical power received at output λ_2 as a function of input RF frequency with only λ_3 and λ_4 used as input wavelengths. Fig. 5(b) shows the output on λ_2 with λ_3, λ_4, and λ_7 used as inputs. It is immediately evident that the forms of the two responses are very similar. Both measurements clearly oscillate with the input RF frequency with a period of approximately 24 GHz, which corresponds well with the nominal differential delay of 40 ps between λ_3 and λ_4. The attenuation observed with increasing frequency can be attributed primarily to the frequency response of the optical modulator and RF cables used in the system (as presented in the Appendix).

It can also be seen that the net optical power received at λ_2 is different when two and three wavelengths are used—Fig. 5(a) and (b), respectively. This can be explained due to our decision to maintain the total optical power as constant at the input to the HNLF, resulting in a two-thirds reduction in the power of each carrier when going from two to three input wavelengths.

Similarly to Fig. 5(a) and (b), Fig. 5(c) presents the power measurements at λ_1 as a function of input RF frequency with only λ_4 and λ_7 input to the system. Fig. 5(d) presents the optical power measured at λ_1 with λ_3, λ_4, and λ_7 used as inputs. Again, very similar responses are observed for both cases. The output at λ_1 oscillates with input frequency with a period of approximately 8 GHz, which agrees well with the nominal delay of 120 ps between λ_4 and λ_7. Again, when comparing the two- and three-wavelength cases, a reduction in net optical power output at λ_1 is observed due to the reduction in pump power per channel for the case of three input wavelengths.

Fig. 5(a)–(d) also present the predicted responses achieved using (2) and the parameters extracted from the system characterization and calibration presented in the Appendix. Excellent agreement between the theoretical prediction and measured response is achieved in all four experiments. It should be noted that no variation of the ACF of (2) was conducted to achieve this remarkable match between prediction and experiment. This proves that (2) is equally applicable in the case of three input wavelengths as it is for two inputs. Further, this accurate matching of prediction and experiment also verifies that we can achieve two independent ACFs simultaneously and in parallel with the system of Fig. 4.

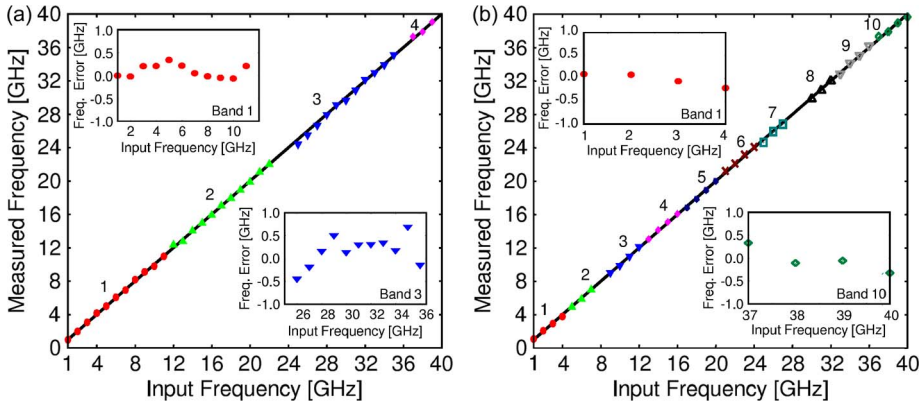

Fig. 6. Interpreted frequency by solving (2) using the measured DC voltages of Fig. 5. (a) Solving data of Fig. 5(b), assuming four unambiguous measurement bands. (b) Solving data of Fig. 5(d), assuming 10 unambiguous measurement bands. (Insets) Plot frequency errors at selected bands. Solid lines are ideal results with no error, and dots are measurements.

Having established that (2) provides an accurate ACF, we can use this equation to interpret the IFM output as a frequency measurement. Provided the RF signal power is known, the system response is fully determined for a given selection of mixing wavelength channels. To measure the frequency of the RF signal, (2) is solved to map the voltage to interpreted frequency. Since (2) is oscillatory in nature, a band of operation must be assumed in order to obtain a one to one mapping hence achieve unambiguous measurement.

Fig. 6 present the interpreted frequency obtained by solving (2) using the measurement values of Fig. 5. Fig. 6(a) has four distinct bands where mapping from voltage to frequency is unambiguous. Similarly, Fig. 6(b) has 10 distinct bands as the function has more oscillations due to the longer differential time delay between the mixing channels. The interpreted frequencies are very close to the ideal values indicated by a solid line, with an error estimated within $+/-500$ MHz achieved over the entire measurement band of 1–40 GHz, with larger errors observed at the edges of each band, as expected. The photonic IFM with simultaneous multiple measurements in a single HNLF was thus been successfully demonstrated.

6. Discussion and Conclusion

We have shown that the all-optical frequency measurement system of [6] can be extended to achieve multiple independent IFM implementations without significantly increasing the cost or complexity of the optical fiber system. This represents a significant step toward the realization of a practical, all-optical frequency measurement system that is competitive in terms of performance with contemporary electronic systems [8] but requires no high-speed electronic components and can be easily extended to operation bandwidth of 1–40 GHz or beyond.

In this specific demonstration, two different IFM responses were achieved using a single optical modulator, CFBG, EDFA, and HNLF. A third IFM can be added by simply monitoring the mixing product between λ_3 and λ_7. Further IFMs could be introduced by adding extra wavelengths, but care would need to be taken to ensure that the resulting mixing products did not overlap, placing some constraints on the combinations of wavelength channels that can be used. It is proposed that an alternate method of *labeling* the various mixing products may be conceived rather than relying on their wavelengths. One possibility would be to modulating each optical carrier by a distinct low-frequency dither tone. This would enable isolation of idlers using dither tones that they inherit from their pumps and enable phased-locked-loop techniques to be employed with consequent improvements to sensitivity [9]. Investigation of such alternate labeling techniques is currently underway. We are also in the process of quantifying the system stability, sensitivity, frequency measurement range, dynamic range, and overall system cost and will assess the impact of implementing multiple IFM systems simultaneously on these system characteristics.

To claim that an IFM system has been fully implemented, it would be necessary to provide orthogonal sine and cosine measurements such that both the amplitude and frequency of the signal to be measured can be identified simultaneously and unambiguously. This requires the use of a Hilbert transform in one arm of the IFM. We have demonstrated techniques to achieve this photonically [10] and have applied this technique to an IFM system [11]. We are currently exploring system topologies that can utilize the current demonstrated simultaneous parallel IFM approach to achieve such an amplitude independent IFM implementation.

Appendix

The effectiveness of our IFM system relies on our ability to use (1) to predict the output optical power that will result for a given input RF frequency. However, in order to use (1) effectively, a number of aspects of the system must be characterized and calibrated.

To assist with this process, we rearrange and simplify (1) by assuming that effects of dispersion are insignificant. This is valid since the HNLF exhibits very low dispersion at its operation wavelengths, and the optical carrier wavelengths have been chosen to be close to the center of the reflection bands of the CFBG. We also factor out the carrier amplitude A to obtain

$$P(\lambda_{\text{Idler}}) \propto 1 + 2m^2(f)[5 + 4\cos(2\pi f \Delta t)] \tag{2}$$

where $\Omega = 2\pi f$, and we have defined the modulation index as $m(f) = B/A$. This modulation index is a measure of the strength of RF modulation achieved by the Mach–Zehnder modulator, including both the strength of the input RF power and the efficiency of the modulator, and is frequency dependent due to the degrading efficiency of the modulator at high frequency. To proceed, it will be valuable to characterize the frequency response of the modulator and, hence, obtain an empirical measure of $m(f)$.

A.1. Predicted Frequency Response of the Optical Power Output from the MZM

Typically, the frequency response of an MZM is measured by assembling a high-frequency photonic link consisting of modulator, fiber link, and broadband photodetector [12]. The response of this link is then measured using a network analyzer, and the modulator response is de-embedded from the full photonic link. In our case, no high-speed photodetector is used, and thus, an alternate technique which uses the DC optical outputs is more appropriate.

The optical intensity at the output of an MZM I_{MZM} can be expressed as

$$I_{\text{MZM}} = 0.5P_{\text{opt}}\{1 + \cos[m(f)\cos(2\pi ft) + \phi]\} \tag{3}$$

where P_{opt} is the input optical power, ϕ is the phase shift between the two arms of the Mach–Zehnder, which can be controlled using a DC bias voltage, and $m(f)$ is the frequency dependent modulation index that we wish to characterize. Expanding I_{MZM} as a Bessel series, and retaining only the DC terms, we get

$$I_{\text{MZM}}(DC) = 0.5P_{\text{opt}}\{1 + J_0[m(f)]\cos(\phi)\}. \tag{4}$$

From (4), it is clear that the DC optical power resulting at the modulator output can be used to characterize the frequency dependent modulation index $m(f)$.

In order to characterize the frequency dependent modulation index of the modulator used in this study, the setup of Fig. 7(a) was configured with all three lasers set to output power of 0 dBm. The modulator DC bias was set to achieve minimum transmitted power, and at the same time, the RF input was driven by an SG with RF power maintained at 10 dBm. The optical power at the modulator output was detected using a low-frequency photodetector, and the resulting voltage was recorded while the input RF was swept from 1–40 GHz. Equation (4) was then used to extract the frequency dependent modulation index $m(f)$, as presented in Fig. 7(b).

Typically, the frequency response of a velocity matched Mach–Zehnder modulator is determined by the conductor losses in the modulating electrode, as well as the cable feeding the

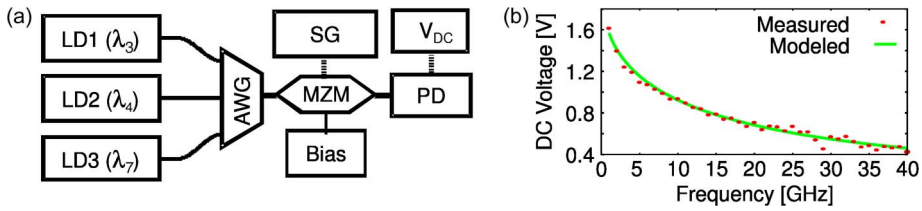

Fig. 7. Characterisation of the modulator frequency response. (a) Experiment setup. (b) Modulator frequency response. (Dots) Measurements. (Solid line) Fitting using (4) and (5).

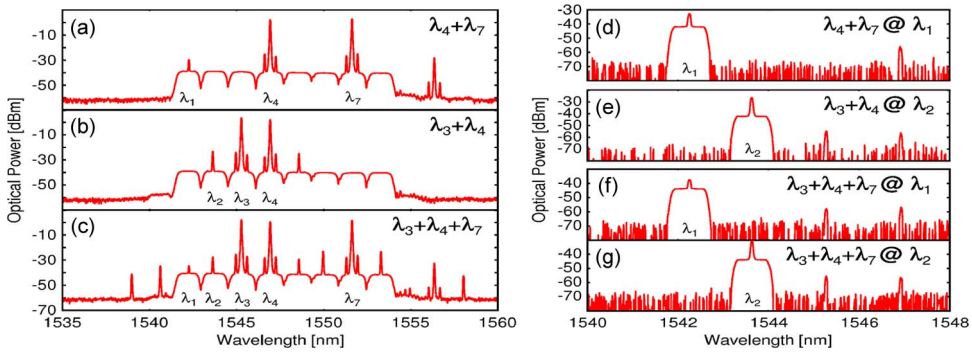

Fig. 8. Optical Spectrum Analyser traces at output of the HNLF [(a)–(c)] and after optical filtering [(d)–(g)]. (a) Mixing of λ_4 and λ_7. (b) Mixing of λ_3 and λ_4. (c) Mixing of all three channels (λ_3, λ_4, and λ_7). (d) Filtered spectrum of (a) through AWG port 1 (λ_1). (e) Filtered spectrum of b) through AWG port 2 (λ_2). (f) Filtered spectrum of (c) through AWG port 1 (λ_1). (g) Filtered spectrum of (c) through AWG port 2 (λ_2).

modulator input [12]. If this is the case, the frequency dependent modulation index can be effectively modeled as

$$m(f) = m_0 e^{-\alpha\sqrt{f}} \tag{5}$$

where m_0 is the DC modulation index, and α is the attenuation constant. It is possible to fit (5) to the measured modulation index of Fig. 7(b) using $m_0 = 0.129$ and $\alpha = 0.136$ $(\text{GHz}^{-0.5})$. This fit is also presented on Fig. 7(b), and it can be seen that the modulator response is well characterized by these parameters.

We have thus characterized the frequency response of the optical modulator. Further, we assert that since all of the other components in the system are either all-optical or operate at DC, the modulator represents the only significant frequency dependence in the system, and thus, $m(f)$ should be sufficient to determine the frequency response of the entire IFM system. This assertion is supported by our previous characterization of the optical components in [6].

A.2. Optical Spectra of the Nonlinear Mixing Products

Having characterized the frequency response of the optical modulator, we must now characterize the mixing efficiency of the HNLF at the wavelengths and powers used in this investigation. To perform this characterization, an optical spectrum analyzer with 0.05-nm resolution was used to measure the optical spectrum at the output of the HNLF for various combination of two and three wavelength channels at the input. These spectra are presented in Fig. 8(a)–(c).

Fig. 8(a) presents the spectrum when only λ_4 and λ_7 are input, and Fig. 8(b) presents the spectrum when only λ_3 and λ_4 are present at the input. Fig. 8(c) presents the spectrum when all three channels (λ_3, λ_4, and λ_7) are input. It is evident that with two input channels only two additional idlers are produced at the sum and difference wavelengths. When all three wavelength channels are

input, many additional idler wavelengths can be found at the output. Among them, idlers at λ_1 and λ_2 result uniquely from the mixing of λ_4 and λ_7 and mixing of λ_3 and λ_4, respectively. The amplified spontaneous emission (ASE) noise is also clearly visible with eight optical bands resulting from the reflection off eight-channel CFBG.

In the IFM implementation, the outputs at λ_1 and λ_2 are isolated using an AWG with 0.8-nm pass-band centered at 1542.25 nm (λ_1) and 1543.65 nm (λ_2). Fig. 8(d) and (e) present the AWG filtered spectra at the output channels λ_1 with inputs on λ_4 and λ_7, and at the output λ_2 with inputs on λ_3 and λ_4, respectively. Fig. 8(f) and (g) present the AWG filtered spectra at the output channels λ_1 and λ_2, respectively, with all three input channels (λ_3, λ_4, and λ_7) present. It is evident that optical filtering has significantly suppressed spectral components outside the filtering pass-band such that the contributions from λ_3, λ_4, and λ_7 [which are very strong in Fig. 8(a)–(c)] have been suppressed by more than 20 dB, relative to the power at λ_1 or λ_2.

From Fig. 8(d)–(g), we have a direct measurement of the output optical power that can be expected at the system outputs at λ_1 and λ_2 for given configurations of optical inputs λ_3, λ_4, and λ_7. This information can be used to calibrate both the nonlinear optical mixing efficiency, as well as the photodetector response.

A.3. Calibration of Amplification, Nonlinear Mixing, Filtering, and Detection

Equation (2) shows that the output optical power will be proportional to an oscillating function of the input RF frequency. To actually use (2) for frequency measurement, it is necessary to determine the constant of proportionality. This constant factor will include the effects of amplification, nonlinear mixing, and losses in the CFBG, and AWG filters. Further, the output of the DC photodetector is a *voltage* which is proportional to the detected optical power. We wish to use this output voltage to determine the input RF and thus we also need to calibrate the efficiency of the photodetector. Since we have asserted that amplification, nonlinear mixing, filtering, and differential delays and the DC photodetection will provide repeatable responses that are independent of RF frequency, we can combine all of these effects in a simple calibration factor. For brevity, this calibration factor will be calculated independently for each different combination of input optical wavelength and power in Fig. 8.

To determine the calibration factor for each investigated combination of input wavelengths, the system was configured as presented in Fig. 4 under the conditions described to achieve Fig. 8(d)–(g). The RF input signal was turned off, and the output voltages from the DC photodetector were recorded for each wavelength combination of Fig. 8(d)–(g). By setting the RF power to zero, the modulation index is also zero, and thus, $m(f) = 0$, reducing (2) to the trivial expression $P(\lambda_{\text{Idler}}) \propto 1$. Thus, the measurement of optical power with the RF input set to zero amplitude will in fact yield the constant of proportionality required to calibrate the system.

For each of the cases of Fig. 8(d)–(g), the measured output voltages with no input RF signal were 0.498, 0.939, 1.125, and 2.290 V, respectively, and thus, these can be used as the calibration factors to scale (2). These are the actual calibration factors used in Section 5 and Fig. 5.

References

[1] H. Cuckson and P. D. Curtis, "Microwave instantaneous frequency measurement apparatus," U.S. Patent 4 414 505, Nov. 8, 1983.
[2] G. Liang, C. Shih, R. Withers, B. Cole, M. Johansson, and L. Suppan, Jr., "Superconductive digital instantaneous frequency measurement subsystem," *IEEE Trans. Microw. Theory Tech.*, vol. 41, no. 12, pp. 2368–2375, Dec. 1993.
[3] L. Nguyen and D. Hunter, "A photonic technique for microwave frequency measurement," *IEEE Photon. Technol. Lett.*, vol. 18, no. 10, pp. 1188–1190, May 2006.
[4] N. Sarkhosh, H. Emami, L. Bui, and A. Mitchell, "Reduced cost photonic instantaneous frequency measurement system," *IEEE Photon. Technol. Lett.*, vol. 20, no. 18, pp. 1521–1523, Sep. 2009.
[5] L. Nguyen, "Microwave photonic technique for frequency measurement of simultaneous signals," *IEEE Photon. Technol. Lett.*, vol. 21, no. 10, pp. 642–644, May 2009.
[6] L. Bui, M. Pelusi, T. Vo, N. Sarkhosh, H. Emami, B. Eggleton, and A. Mitchell, "Instantaneous frequency measurement system using optical mixing in highly nonlinear fiber," *Opt. Exp.*, vol. 17, no. 25, pp. 22 983–22 991, Dec. 2009.

[7] N. Sarkhosh, H. Emami, L. Bui, and A. Mitchell, "Microwave photonic instantaneous frequency measurement with simultaneous parallel operation within a single optical fiber," in *Proc. IEEE IMS*, Anaheim, CA, May 2010, pp. 368–372.
[8] Instantaneous Frequency Measurement Receiver Systems (IFM). [Online]. Available: http://www.widebandsystems.com/ifm.html
[9] N. Sarkhosh, H. Emami, L. Bui, and A. Mitchell, "Microwave photonic instantaneous frequency measurement with improved sensitivity," in *Proc. IEEE IMS*, Boston, MA, Jun. 2009, pp. 165–168.
[10] H. Emami, N. Sarkhosh, L. Bui, and A. Mitchell, "Wideband RF photonic in-phase and quadrature-phase generation," *Opt. Lett.*, vol. 33, no. 2, pp. 98–100, Jan. 2008.
[11] H. Emami, N. Sarkhosh, L. Bui, and A. Mitchell, "Amplitude independent RF instantaneous frequency measurement system using photonic Hilbert transform," *Opt. Exp.*, vol. 16, no. 18, pp. 13 707–13 712, Sep. 2008.
[12] G. Gopalakrishnan, W. Burns, R. McElhanon, C. Bulmer, and A. Greenblatt, "Performance and modeling of broadband $LiNbO_3$ traveling wave optical intensity modulators," *J. Lightw. Technol.*, vol. 12, no. 10, pp. 1807–1819, Oct. 1994.